Particuology 115 (2026) 78–90

Contents lists available at ScienceDirect

Particuology

journal homepage: www.elsevier.com/locate/partic

Controllable microfluidic fabrication of monodisperse PCL microspheres for soft tissue augmentation

Xing-Long Zhou[a], Hao-Wen Zhu[a], Han Fu[a], Chang-Hai Zhou[a], Da-Wei Pan[a,b], Yu-Chao Deng[a], Wei Wang[a,b], Zhuang Liu[a,b], Rui Xie[a,b], Xiao-Jie Ju[a,b,*], Liang-Yin Chu[a,b]

[a] School of Chemical Engineering, Sichuan University, Chengdu, 610065, China
[b] National Key Laboratory of Advanced Polymer Materials, Sichuan University, Chengdu, 610065, China

HIGHLIGHTS

- Monodisperse PCL microspheres with precise size regulation are fabricated via droplet-based microfluidics.
- PCL microspheres exhibit superior long-term stability and excellent biocompatibility.
- Monodisperse 42 μm PCL microspheres exhibit the most superior ability to stimulate collagen neogenesis.

GRAPHICAL ABSTRACT

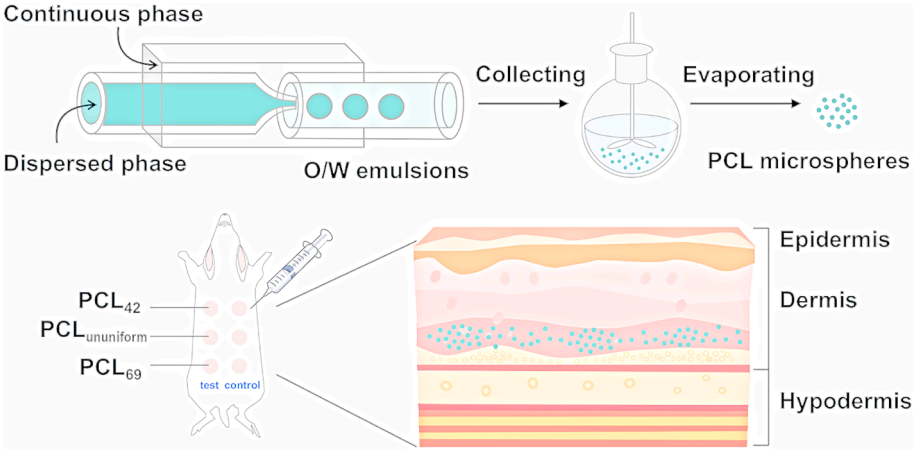

ARTICLE INFO

Keywords:
Polycaprolactone
Microfluidics
Monodisperse microspheres
Collagen regeneration

ABSTRACT

Polycaprolactone (PCL) microspheres are emerging as versatile biomaterials for minimally invasive soft tissue augmentation due to their tunable biodegradability and favorable biocompatibility. Nevertheless, the extent to which monodispersity governs the functional performance of PCL microspheres, particularly in modulating host tissue responses and regenerative efficacy, remains poorly understood. Herein, we propose a method to controllably prepare monodisperse oil-in-water (O/W) droplet templates using coaxial flow-focusing microfluidics, and then obtaining monodisperse PCL microspheres with programmable sizes via solvent evaporation. The droplet dimensions are inversely regulated by the outer-to-inner phase flow rate ratio, while PCL concentration in the organic phase exerts minimal influence on initial droplet size but markedly reduces the volume shrinkage during solidification, yielding microspheres that better retain their geometries. Notably, the resultant PCL microspheres can maintain structural integrity and size uniformity over two-month period under physiologically mimetic conditions. Comprehensive biocompatibility assessments reveal that PCL microspheres exhibit

This article is part of a special issue entitled: SI honoring Profs. Jin & Yu published in Particuology.

* Corresponding author. School of Chemical Engineering, Sichuan University, Chengdu, 610065, China.
E-mail address: juxiaojie@scu.edu.cn (X.-J. Ju).

https://doi.org/10.1016/j.partic.2026.04.027
Received 2 January 2026; Received in revised form 25 March 2026; Accepted 27 April 2026
Available online 13 May 2026

negligible hemolytic activity and cytotoxicity, demonstrating excellent hemocompatibility and cytocompatibility. Notably, in a rabbit soft tissue implantation model, monodisperse PCL microspheres with an average diameter of 42 μm elicit attenuated foreign body reactions and potentiate endogenous collagen deposition relative to the polydisperse microsphere control group. These results provide useful guidance for the application of PCL microspheres in soft tissue augmentation.

1. Introduction

In the fields of medical aesthetics and reconstructive surgery, soft tissue augmentation plays a crucial role in restoring volume deficits and correcting facial/dermal depressions and wrinkles, which predominantly relies on biocompatible implantable materials (Bai et al., 2025; Minokadeh & Kakar, 2025; Kontis, 2013). As the primary component of the skin's extracellular matrix, collagen not only endows the dermis with mechanical integrity but also contributes to skin elasticity and youthful appearance through continuous remodeling (Herrmann et al., 2018). Unfortunately, age-related or trauma-induced imbalances in collagen metabolism, characterized by reduced synthesis and increased degradation, undermine these functions, manifesting as skin sagging and wrinkles (Carretero et al., 2023; Nakamura et al., 2021; Shin, Jang, et al., 2019; Varani et al., 2006). Subcutaneous fillers are classified into permanent (e.g., polymethyl methacrylate, polyacrylamide hydrogel) and non-permanent (e.g., hyaluronic acid, collagen) types. They can effectively restore facial volume and correct contours, but have obvious limitations. Permanent fillers, despite their durability, pose risks of severe complications including inflammatory nodules, leading to a preference for non-permanent options (Requena et al., 2011). Conversely, current non-permanent fillers, which function primarily through passive volume replacement, suffer from transient efficacy due to rapid biodegradation, requiring repeated treatments (Seong et al., 2019; Choi et al., 2018; Jeong et al., 2016; Hua et al., 2020; Yan et al., 2024). To overcome these drawbacks, materials that can effectively and sustainably stimulate endogenous collagen regeneration have become a research focus (Gao et al., 2021; Li, Xu, et al., 2024; Pan et al., 2022).

Bio-stimulatory soft tissue fillers, such as polycaprolactone (PCL), poly-L-lactic acid (PLLA), and calcium hydroxylapatite (CaHA), exert their effects by eliciting a foreign body response that activates dermal fibroblasts to produce collagen and counteract age-related volume loss (Gao et al., 2021; Hwang et al., 2021). Of these, microspheres made from PCL confer a unique advantage in terms of durability due to their prolonged degradation profile (2-4 years), which is superior to that of PLLA and CaHA under the same subcutaneous microenvironment (Ikada & Tsuji, 2000; Shin, Jang, et al., 2019). Despite the potential of PCL microspheres for soft tissue filling and collagen induction, their clinical performance is intricately linked to their physical characteristics, particularly particle size and monodispersity. Critical challenges persist: undersized microspheres are prone to rapid clearance by macrophages, leading to heightened lymphocytic infiltration and neovascularization; conversely, oversized or polydisperse microspheres elicit excessive inflammatory responses (Chikaura et al., 2016; Hossain et al., 2015). These observations underscore a compelling need to systematically elucidate how the monodispersity and specific size of PCL microspheres regulate inflammatory responses and collagen regeneration.

Current methods for fabricating PCL microspheres, such as homogeneous emulsification, spray drying, and nanoprecipitation, often suffer from limitations in terms of precise size control, poor batch-to-batch consistency, and irregular morphology (Deliormanli & Yenice, 2021; Yan et al., 2022; Jang et al., 2020; Fan & Jin, 2015; Wang et al., 2018). While PCL microspheres have been used as filling materials to promote collagen regeneration in previous studies (Cao et al., 2025; Xie et al., 2025), there is a lack of a systematic investigation into how PCL microsphere size and monodispersity affect their ability to enhance collagen regeneration. Microfluidic droplet-based approaches offer distinct advantages by enabling precise manipulation of fluids at the micro/nanoscale, thereby facilitating the generation of monodisperse microspheres via the controlled formation of monodisperse droplet templates (Chu et al., 2007; Jiang et al., 2023; Long et al., 2024; Wen et al., 2023; Yang et al., 2024). Herein, leveraging a coaxial glass capillary microfluidic device (Fig. 1), we utilize a polyvinyl alcohol (PVA) aqueous solution as the outer (continuous) phase and a PCL/dichloromethane (DCM) solution as the inner (dispersed) phase. Monodisperse oil-in-water (O/W) droplet templates are formed at the microfluidic orifice due to shear forces exerted by the outer phase; these droplets are subsequently solidified into monodisperse PCL microspheres. We systematically investigate the influence of the outer-to-inner phase flow rate ratio (Q_o/Q_i) on O/W droplet size and explore the relationships between the PCL concentration in the inner phase and the dimensions of droplets and microspheres, as well as the droplet-to-microsphere diameter shrinkage ratio. Furthermore, the *in vitro* stability and biocompatibility of the prepared PCL microspheres are thoroughly evaluated. Finally, *in vivo* animal studies are conducted to assess the impact of PCL microsphere size parameters on localized inflammatory responses and the induction of collagen regeneration. The novelty of this study lies in the fabrication of monodisperse PCL microspheres with precisely controllable particle size using a coaxial microfluidic method for subcutaneous tissue filling, and the establishment of a precise microsphere size control method. The effect of particle size uniformity versus heterogeneity, as well as absolute particle size on collagen regeneration stimulation are systematically investigated, providing theoretical guidance for the application of PCL microspheres in the fields of soft tissue filling.

2. Experimental

2.1. Materials

PCL (Mn = 50000-60000), PVA (PVA-1799), mannitol, and sodium carboxymethyl cellulose (CMC) are purchased from Shanghai Aladdin Reagent Co., Ltd. PBS (pH 7.4) and DMEM medium are purchased from Gibco Ltd. Sodium citrate rabbit whole blood is purchased from Chengdu Dasuo Laboratory Animal Co., Ltd. L929 mouse fibroblast cells are purchased from the Beijing Cell Bank of the Chinese Academy of Sciences. For evaluating the biocompatibility of the microspheres, relevant biological reagents are purchased from Beyotime Biotechnology.

2.2. Precision fabrication of monodisperse PCL microspheres

Monodisperse PCL microspheres are fabricated using a coaxial co-flow microfluidic device assembled from glass capillaries. The device consists of a glass slide, a pulled-and-polished injection tube (550/960 μm ID/OD capillary with a 60 μm flat orifice), a collection tube (200/960 μm ID/OD capillary), and interconnecting square capillary and blunt needles.

Size control of O/W droplet templates and PCL microspheres is achieved by regulating the outer-to-inner phase flow rate ratio ($Q_o/Q_i = 2\sim10$). The continuous phase is a 5 wt% PVA aqueous solution, and the dispersed phase is a PCL/DCM solution. In addition, the impact of PCL concentration (1∼5 wt% in DCM) on droplet and microsphere sizes is investigated. Resultant droplets and microspheres are imaged using an industrial microscope. Quantitative size analysis is performed by measuring 100 particles per sample, and the coefficient of variation

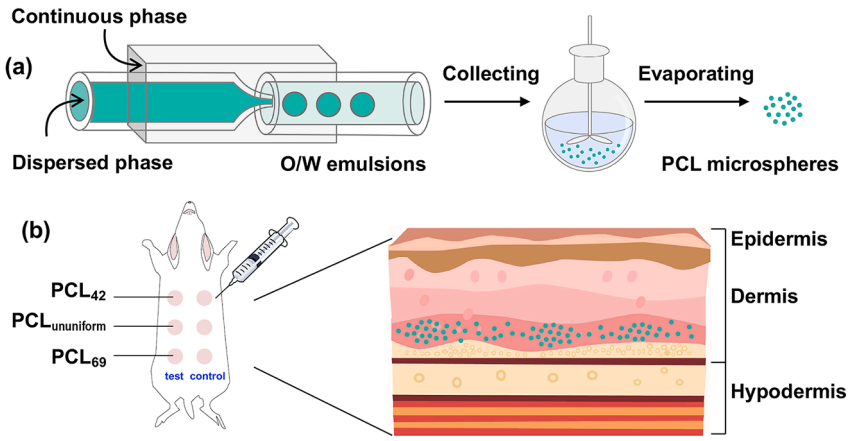

Fig. 1. Schematic illustrations of the fabrication process of PCL microspheres by microfluidics (a) and *in vivo* experiments with PCL microspheres stimulating collagen regeneration.

(CV), as defined by Equation (2–1), is used to assess their monodispersity.

$$CV(\%) = \frac{1}{\bar{d}}\left[\sum_{i=1}^{n}\frac{(d_i-\bar{d})^2}{n}\right]^{\frac{1}{2}} \times 100\% \tag{2-1}$$

here, n represents the total number of analyzed particles (droplets or microspheres), d_i is the diameter of the i-th individual particle, and d is the arithmetic mean diameter, calculated as the average of all d_i values.

Furthermore, to establish a quantitative relationship between the initial droplets and the final solidified microspheres, the dimension change is characterized by the droplet-to-microsphere shrinkage ratio (SHR), which quantifies the shrinkage extent during solvent evaporation and solidification, defined by Equation (2–2).

$$SHR = \frac{D_e - D_p}{D_e} \times 100\% \tag{2-2}$$

here, D_e represents the average diameter of the initial droplet, while D_p corresponds to the diameter of the final solidified microsphere.

The morphological evolution of PCL microspheres during solvent evaporation is intricately linked to the concentration-dependent phase separation behavior of PCL. To elucidate the influence of PCL concentration on microstructural characteristics, a systematic investigation is conducted. Using a fixed outer-to-inner phase flow rate ratio ($Q_o/Q_i = 10$), PCL microspheres are fabricated with varying PCL concentrations (1, 3, and 5 wt%) in the dispersed phase. After solidification, the microspheres are collected, washed to remove residual solvents and surfactants, and subsequently freeze-dried to preserve their native structure. The resulting microspheres are then observed using scanning electron microscopy (SEM) to characterize their microstructures. For PCL42, the outer phase flow rate is 80 μL/min and the inner phase flow rate is 16 μL/min; for PCL69, the outer phase flow rate is 40 μL/min and the inner phase flow rate is 20 μL/min; for heterogeneous PCL, the outer phase flow rate ranges from 40 to 200 μL/min and the inner phase flow rate ranges from 1 to 30 μL/min. Dichloromethane is evaporated at ambient temperature with stirring at 300 rpm for 2 h. The total volume of the injected liquid is 0.2 mL, and the particle concentration during injection is 300 mg/mL.

2.3. Fabrication and morphological characterization of polydisperse PCL microspheres

For comparative analysis against the monodisperse counterparts, we also use droplet microfluidics to intentionally prepare polydisperse PCL microspheres as a control group, aiming to assess how size dispersity influences their *in vivo* functionality. While maintaining a 5 wt% PVA solution as the continuous phase and PCL/DCM solutions (1, 3, 5 wt%) as the dispersed phase, we dynamically vary the flow rates of the two phases during droplet generation. This method of applying non-uniform hydrodynamic shear deliberately results in the formation of droplets with a wide size distribution, which finally form polydisperse microspheres upon solvent evaporation. The size heterogeneity is confirmed by imaging via an industrial microscope. The washed and freeze-dried polydisperse PCL microspheres are characterized via SEM.

2.4. Evaluation of the in vitro stability of PCL microspheres

To evaluate the particle stability and integrity of prepared PCL microspheres, we conduct an *in vitro* stability assay. Three types of microspheres are tested: monodisperse PCL_{42} microspheres (average diameter = 42 μm, CV = 4.2%), monodisperse PCL_{69} microspheres (average diameter = 69 μm, CV = 3.1%), and polydisperse $PCL_{nonuniform}$ microspheres (average diameter = 46 μm, CV = 41.6%). After freeze-drying, the microspheres are suspended in PBS (pH 7.4) and incubated in an air-bath shaker at 37 °C with shaking at 100 rpm. Samples are collected at 0, 1, 2, 4, 6, and 8 weeks, washed, freeze-dried again, and their morphological changes are characterized by SEM.

2.5. Comprehensive biocompatibility assessment of PCL microspheres

2.5.1. Hemolysis assay of PCL microspheres

The hemolytic potential of PCL microspheres is assessed using a rabbit blood model. Rabbit blood is diluted with normal saline and centrifuged repeatedly until plasma is completely removed to prepare a 2 wt% red blood cell (RBC) suspension. PCL microsphere dispersions (50 to 1000 μg/mL) are prepared, with normal saline as the negative control and deionized water as the positive control. To each 2 mL tube, 0.5 mL of sample or control is added and pre-warmed at 37 °C for 30 min, followed by the addition of 0.5 mL of RBC suspension and an additional 1 h incubation. After incubation, samples are centrifuged. The visual appearance of the supernatant is recorded, and 200 μL of the supernatant is sampled to measure the absorbance at 540 nm to determine the degree of hemolysis.

2.5.2. Coagulation assay of PCL microspheres

The thrombogenic potential of PCL microspheres is evaluated via a combined qualitative and quantitative coagulation assay. In the qualitative assay, PCL microsphere dispersions and the normal saline control (50 μL each) are added to a 96-well plate. A blood/$CaCl_2$ mixture is added to initiate coagulation, and coagulation formation is photographed at 1, 3, 5, 7, and 10 min post-initiation after washing with normal saline. Quantitatively, PCL microsphere dispersions and the

normal saline control (50 μL each) are added to tubes (5 replicates per group). After adding the blood/$CaCl_2$ mixture and incubating at 37 °C for 10-50 min, coagulation is terminated by adding 4 mL of deionized water. Following lysis of the unclotted RBCs, the absorbance of the supernatant (OD_{540}) is measured to determine the coagulation degree.

2.5.3. Cytocompatibility evaluation of PCL microspheres

The cytocompatibility of PCL microspheres is evaluated using the CCK-8 assay with L929 mouse fibroblasts. L929 cells are seeded into 96-well plates (2×10^4 cells per well). After 24 h of incubation, the culture medium is replaced with PCL microsphere suspensions (50 to 1000 μg/mL, sterilized by UV irradiation). After an additional incubation for 24, 48, and 72 h, CCK-8 reagent (diluted 1:10 in culture medium) is added to each well. After incubation for 1-3 h, the absorbance at 450 nm is measured to assess cell viability.

2.6. PCL microsphere-mediated in vivo collagen neogenesis

2.6.1. Animal model establishment

All animal experimental procedures in this study are approved by the Animal Ethics Committee of Sichuan Linisonuo Biotechnology Co., Ltd. (LLSW-2024172).

A total of 20 healthy female New Zealand White rabbits (weighing 2.0-2.5 kg, aged 3 months) are selected for this study. To minimize inter-individual variability, a parallel split-dorsal implantation design is employed. Specifically, three distinct injection sites are chosen on the dorsum of each rabbit, ensuring that the sites are sufficiently spaced to prevent cross-interference. Animals are randomly assigned, and at each predetermined time point (1, 2, 4, 8, 12, and 24 weeks post-implantation), three randomly selected rabbits are euthanized to harvest specimens for subsequent analysis.

Post-operatively, all animals are housed individually in cages under strict hygienic conditions. Clinical observations are performed daily for the first post-implantation week and weekly thereafter. Observations focus on the skin overlying the implantation sites for signs of erythema, edema, or ulceration. General health is monitored by assessing the animals' mental status, food/water intake, locomotor activity, and presence of abnormal secretions. Body weight is recorded weekly to monitor overall health status.

2.6.2. Histopathological examination

Skin samples from injected and control sites are harvested at 1, 2, 4, 8, 12, and 24 weeks post-implantation (n = 3 per time point). Specimens are fixed in 10% neutral buffered formalin, processed into paraffin blocks, and sectioned for H&E staining. Whole-slide images are captured using a Pannoramic 250 scanner. Low-magnification images are used for general morphology assessment, while 100 × and 400 × images of targeted regions are acquired for histopathological analysis. A semi-quantitative assessment of inflammation and collagen deposition is performed using a four-point scoring scale.

2.6.3. Measurement of dermal thickness

At each post-implantation time point (1, 2, 4, 8, 12, and 24 weeks), dermal thickness is quantified from H&E-stained histological sections using a standardized imaging and measurement protocol. For each experimental sample, 10 independent measurements are manually obtained from distinct dermal regions using CaseViewer analysis software. To determine the net tissue augmentation induced by the microspheres, the mean dermal thickness of the treated area is calculated. Subsequently, the average thickness of the contralateral untreated (blank control) skin from the same animal is subtracted from this value. The final result for each sample represents the mean dermal thickening, serving as a quantitative indicator of the volumetric gain attributable to the implanted microspheres.

2.6.4. Evaluation of collagen deposition by Sirius Red staining

Skin samples are collected at 1, 2, 4, 8, 12, and 24 weeks post-implantation and processed into paraffin sections. After air-drying, sections are stained with Sirius Red solution for 5-10 min, dehydrated, and mounted with coverslips. Images are acquired using a Panthera system. Collagen type differentiation is performed via polarized light microscopy: type I collagen appears bright yellow, and type III collagen appears green.

2.6.5. Evaluation of collagen deposition by Masson's trichrome staining

Skin samples are collected at 1, 2, 4, 8, 12, and 24 weeks post-implantation, processed into sections, and then stained with Masson's Trichrome (Regaud's hematoxylin, Ponceau-Acid Fuchsin, and aniline blue). Images are captured using a 3DHISTECH P250 scanner and Image-Pro Plus 6.0 software is used for quantitative analysis. The fibrosis area percentage is calculated as: (target fiber area/total field area) × 100%.

2.6.6. SEM analysis of the in vivo structural evolution of PCL microspheres

SEM samples are prepared from harvested dermal tissue samples (approximately 0.3 × 0.3 cm^2 in size) at 1, 12, and 24 weeks post-implantation. The excised tissue pieces containing the implants are first rinsed with PBS to remove blood and tissue debris. Subsequently, they are primarily fixed with 2.5% glutaraldehyde in PBS, followed by graded ethanol dehydration. SEM imaging is subsequently performed to evaluate the morphological and surface microstructural changes of the implanted PCL microspheres during *in vivo* residence.

3. Results and discussion

3.1. Controlled preparation and characterization of monodisperse PCL microspheres

Monodisperse PCL microspheres are fabricated through a two-step process: first, generating monodisperse O/W emulsions via microfluidics, followed by solvent evaporation. A key advantage of this method is the precise control over droplet size, achieved by regulating the hydrodynamic parameters in the microfluidic device. The flow rate ratio Q_o/Q_i is systematically varied from 2 to 10 to investigate its effect on emulsion diameter. As shown in Fig. 2(a), a consistent and significant decrease in the average diameter of the O/W emulsions is observed with increasing flow rate ratio, regardless of the PCL concentration in the inner phase (1, 3, or 5 wt%). For instance, at a Q_o/Q_i of 2, the average emulsion diameters are 162 μm, 161 μm and 164 μm for 1 wt%, 3 wt%, and 5 wt% PCL, respectively. At a Q_o/Q_i of 10, the corresponding values decrease to 99 μm, 101 μm and 102 μm, respectively. These results indicate that the droplet formation is primarily controlled by the shear force at the injection tube orifice, which is regulated by the flow rate ratio, whereas the PCL concentration has little effect on the initial droplet size. Notably, all emulsions exhibit narrow size distributions, as shown in Fig. 2(a), confirming the superior monodispersity afforded by the microfluidics.

As shown in Fig. 2(b), the diameters of the solidified microspheres are governed by the synergistic effects of the flow rate ratio Q_o/Q_i and PCL concentration in the inner phase. While increasing the flow rate ratio from 2 to 10 consistently reduces microsphere size across all PCL concentrations, the impact of PCL concentration is far more pronounced. For instance, at the lowest concentration (1 wt% PCL), microspheres with a narrow size distribution exhibit diameters ranging from 25 to 39 μm. However, increasing the PCL concentration to 3 wt% and 5 wt% yields substantially larger microspheres, with average diameters increasing to 33-57 μm and 41-65 μm, respectively. Consequently, a higher PCL concentration within a droplet of a given initial size results in a greater polymer mass, and thus larger microspheres after complete

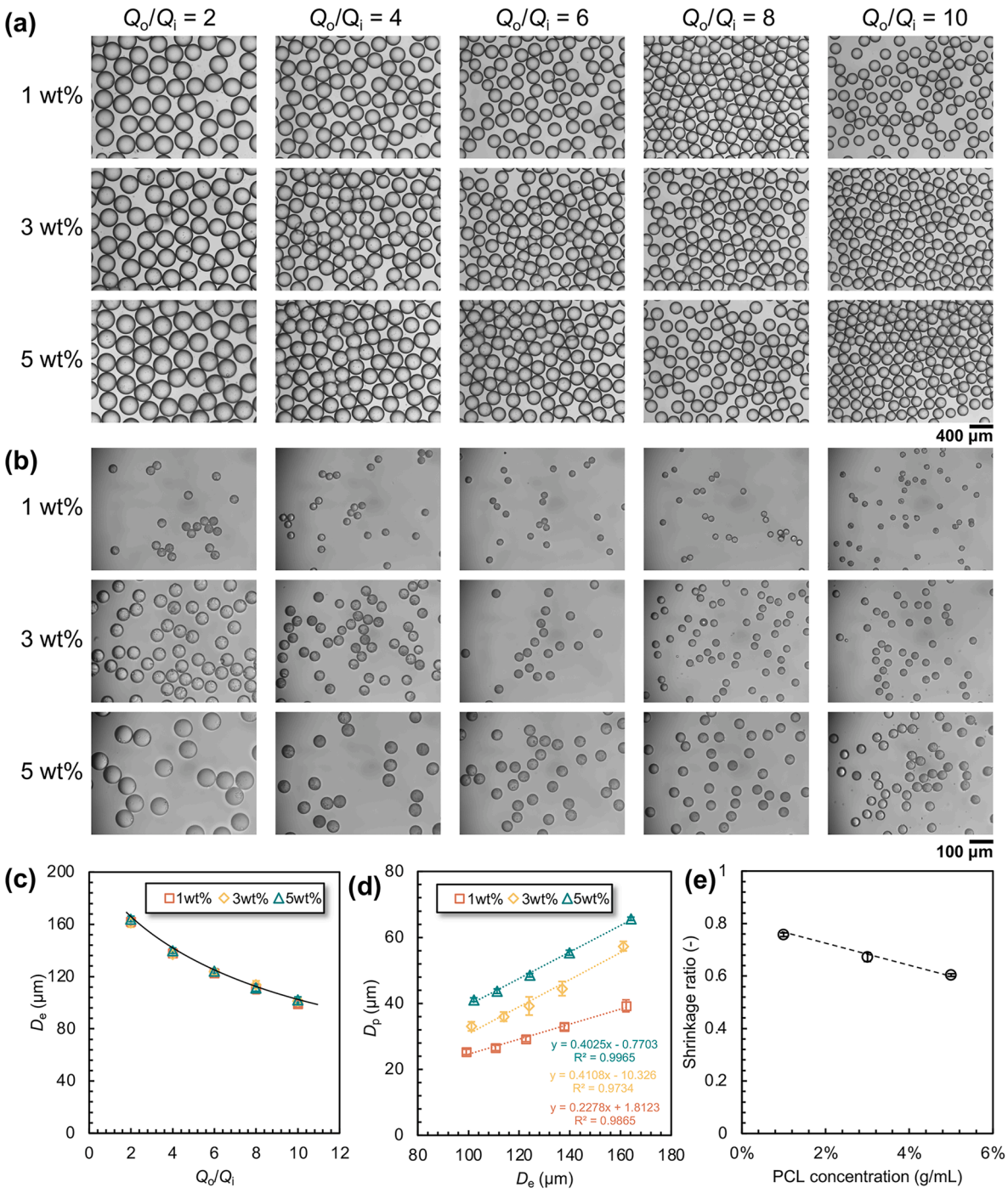

Fig. 2. (a, b) Optical images of PCL emulsions (a) and corresponding microspheres (b) prepared with PCL concentrations of 1 wt%, 3 wt%, and 5 wt% and Q_o/Q_i varying from 2 to 10. (c) Relationship between O/W emulsion diameter and Q_o/Q_i. (d) Relationship between the diameters of emulsions and microspheres. (e) Relationship between PCL concentration and microsphere shrinkage ratio. Data are presented as mean ± SD from three independent experiments for each group.

solvent evaporation and solidification. Notably, throughout this size-tunability study, the prepared microspheres maintain high sphericity and excellent monodispersity, as clearly demonstrated in this figure.

As illustrated in Fig. 2(c), the sizes of both O/W emulsions and the resulting PCL microspheres exhibit a consistent decrease with increasing flow rate ratio Q_o/Q_i. Notably, the magnitude of this size reduction diminishes progressively at higher ratios, suggesting a gradual plateau in the size-tuning sensitivity. In contrast, the initial O/W emulsion droplets show negligible size variation across different PCL concentrations (1 wt %, 3 wt%, and 5 wt%). Furthermore, as shown in Supplementary Fig. S1, the CV values of the emulsions and solidified microspheres are consistently below 5%.

For quantitative prediction, we establish empirical models describing the relationship between the diameter of O/W emulsion droplets (D_e) and the diameter of the solidified PCL microspheres (D_p). Linear fitting of the data, as presented in Fig. 2(d), results in good linear correlations for each PCL concentration. Importantly, these models enable us to calculate the dimensional shrinkage upon solidification. The derived shrinkage ratios (D_e/D_p), defined as the ratio of initial droplet size to final microsphere size, are 75.73%, 67.20%, and 60.36% for 1 wt%, 3 wt%, and 5 wt% PCL, respectively (Fig. 2(e)). This inverse relationship confirms that a higher polymer concentration results in a

reduced volume shrinkage upon solvent evaporation. Most importantly, the existence of these well-defined linear relationships bridges the gap between controlling the easily tunable emulsion droplet size and predicting the final microsphere dimensions.

In addition, the prepared PCL microspheres exhibit structural integrity, excellent sphericity, and high size uniformity. However, subtle morphological variations are observed depending on the PCL concentration. As shown in Fig. S2, at a low concentration of 1 wt%, some microspheres exhibit a distinct porous surface structure. In contrast, microspheres prepared from 3 wt% and 5 wt% PCL solutions are non-porous and feature smooth surfaces.

This concentration-dependent morphological variation can be primarily attributed to differences in the phase separation kinetics of the PCL/DCM system during solvent evaporation. In the low-concentration (1 wt%) system, the lower entanglement density of the PCL molecular chains results in a low-viscosity matrix. This facilitates the formation of localized concentration gradients of the solvent at the air-liquid interface, which effectively drives volatile solvent components to aggregate at specific nucleation sites, thereby inducing pore formation. Conversely, higher PCL concentrations (3-5 wt%) lead to a densely entangled network that suppresses such gradient-driven phase separation, yielding dense, non-porous microspheres (Li et al., 2023). Therefore, by leveraging our microfluidic system for the fabrication of monodisperse O/W emulsion templates, we can now precisely tune and predict the size of the resulting PCL microspheres, thereby achieving a more predictable and controllable fabrication process.

3.2. Characterization of polydisperse PCL microspheres

Polydisperse PCL microspheres are successfully prepared for comparison. As illustrated in Fig. 3, the monodisperse PCL microspheres exhibit excellent size uniformity, with average diameters of 42 μm (Fig. 3(a and b)) and 69 μm (Fig. 3(c and d)), respectively. The polydisperse microspheres exhibit a broad diameter distribution ranging from 10 to 120 μm (Fig. 3(e and f)), with an average diameter of 46.3 μm and a large CV value of 41.6%, which clearly demonstrates their size polydispersity.

Despite the broad size range, the microspheres generally maintain good sphericity. However, notable morphological variations are observed: larger microspheres typically feature crack-marked surfaces, whereas smaller microspheres predominantly exhibit smooth surfaces (Li, Xu, et al., 2024). This size-dependent cracking phenomenon can be

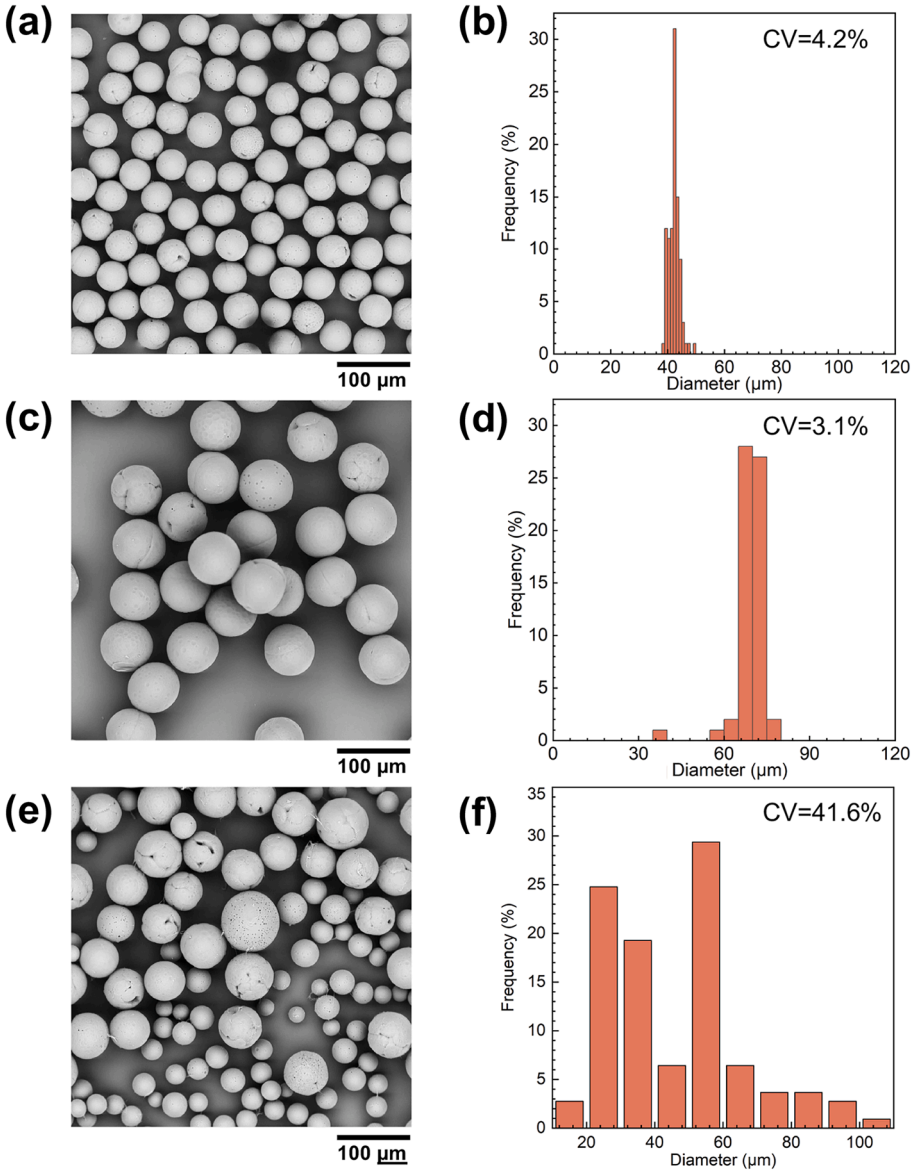

Fig. 3. SEM images (a, c and e) and diameter distributions (b, d and f) of PCL microspheres: (a, b) PCL_{42}, (c, d) PCL_{69}, and (e, f) $PCL_{ununiform}$ microspheres.

attributed to solvent evaporation mechanisms. For larger microspheres, the longer diffusion path for solvent egress from the core to the surface results in more pronounced volumetric shrinkage during solvent evaporation. This induces substantial internal tensile stresses; when these stresses exceed the polymer's mechanical strength at localized points (stress concentration), crack propagation becomes inevitable. Conversely, smaller microspheres, with their higher surface area-to-volume ratio, enable more uniform solvent evaporation and efficient stress relaxation within the polymer matrix, thereby maintaining a smooth surface morphology.

3.3. *In vitro stability assessment of PCL microspheres*

The long-term stability of microspheres is a critical parameter for carrier systems for sustained drug release, tissue engineering scaffolds, and especially soft tissue augmentation applications in aesthetic medicine, where structural integrity must be maintained for at least two months. As shown in Fig. 4, PCL microspheres with varying sizes and size polydispersity maintain excellent structural integrity and sphericity after incubation in PBS for up to 8 weeks (1, 2, 4, 6, and 8 weeks). No structural defects such as cracks, pits, or voids are observed on their surfaces, and their dimensions remain negligibly changed. These observations collectively demonstrate the long-term stability of the fabricated PCL microspheres.

This good stability is primarily attributed to the intrinsic hydrophobicity and highly ordered crystalline structure of PCL, which synergistically inhibit the ingress and subsequent permeation of water molecules. Consequently, the demonstrated physicochemical stability and structural resilience of our microspheres highlight their great potential as durable biomaterials for soft tissue augmentation.

3.4. *In vitro biocompatibility evaluation of PCL microspheres*

Given the potential for intravascular administration or accidental blood exposure for our target applications, a hemocompatibility evaluation is deemed indispensable. As demonstrated in Fig. 5(a), the hemolytic potential among the test groups is readily distinguishable. The positive control group, treated with a detergent, exhibits a characteristic red supernatant following centrifugation, with a visible pellet of residual RBCs at the bottom. This macroscopic observation unequivocally confirms complete hemolysis. In stark contrast, both the negative control (PBS) and all PCL microsphere treatment groups, regardless of concentration, exhibit colorless and transparent supernatants with a compact RBC pellet settling at the bottom. This indicates that no hemolysis occurs in these samples. Quantitatively, the hemolysis rate of all experimental groups is below 1%. This exceptionally low hemolysis rate confirms that the PCL microspheres do not compromise the integrity of RBCs, demonstrating their excellent hemocompatibility.

Furthermore, the coagulation-related properties of the PCL microspheres are assessed using coagulation time tests and the more quantitative blood clotting index (BCI) assay. As shown in Fig. 5(b), the whole blood coagulation time among the experimental groups (blood incubated with PCL microspheres) and the control groups is consistent. For all groups, no clot formation is observed at 1 and 3 min post-incubation, while complete coagulation occurs within the 5-10 min timeframe.

Complementing this qualitative observation, the quantitative BCI analysis presented in Fig. 5(c) reveals that after incubating blood with PCL microspheres at various concentrations for 10-50 min, the BCI values consistently remain above 90%. According to ISO hemocompatibility standards, a BCI value exceeding 90% indicates that the materials do not interfere with the normal hemostatic process. Therefore, our data conclusively demonstrate that PCL microspheres do not adversely affect blood coagulation.

In addition, we evaluate assess the potential cytotoxicity of PCL microspheres toward mammalian cells using the CCK-8 assay. L929 murine fibroblasts, a standard cell line for *in vitro* cytotoxicity screening, are incubated with varying concentrations of PCL microspheres. Strikingly, as shown in Fig. 5(d), cell viability remains above 90% at all time points (24, 48, and 72 h) across all microsphere concentrations. This result confirms that our PCL microspheres are non-cytotoxic. The absence of a dose-dependent decrease in viability suggests that the microspheres exert minimal direct cytotoxic effects on cell membranes, thereby ensuring high cell survival rates.

Collectively, the data from hemolysis, coagulation, and cytocompatibility assessments provide compelling and comprehensive evidence of the excellent overall *in vitro* biocompatibility of our PCL microspheres. This favorable safety profile strongly validates their potential for translational application across diverse biomedical fields, especially those involving direct implantation or injection into the body.

3.5. *In vivo evaluation of collagen neogenesis by PCL microspheres*

3.5.1. *General health and local tolerance in rabbit models after PCL microsphere implantation*

Following subcutaneous injection, all three groups (PCL_{42}, PCL_{69}, and $PCL_{ununiform}$) exhibit typical acute-phase inflammatory responses at the injection site, characterized by erythema (redness) and edema (lump/nodule), on day 1. The resolution kinetics of these inflammatory reactions differ among the three groups. For the monodisperse PCL_{42} group, erythema and edema completely resolve by day 6 and week 3,

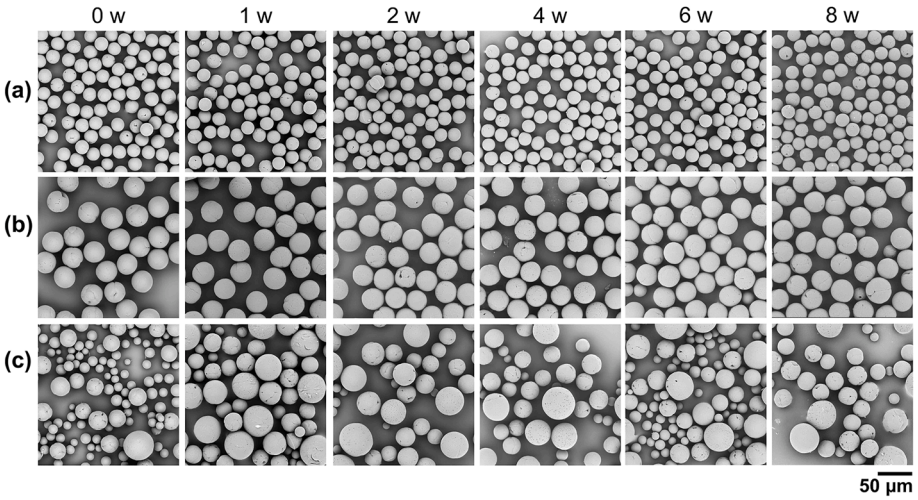

Fig. 4. SEM images of different PCL microspheres incubated in PBS for 0, 1, 2, 4, 6, and 8 weeks: (a) PCL_{42}, (b) PCL_{69}, and (c) $PCL_{ununiform}$ microspheres.

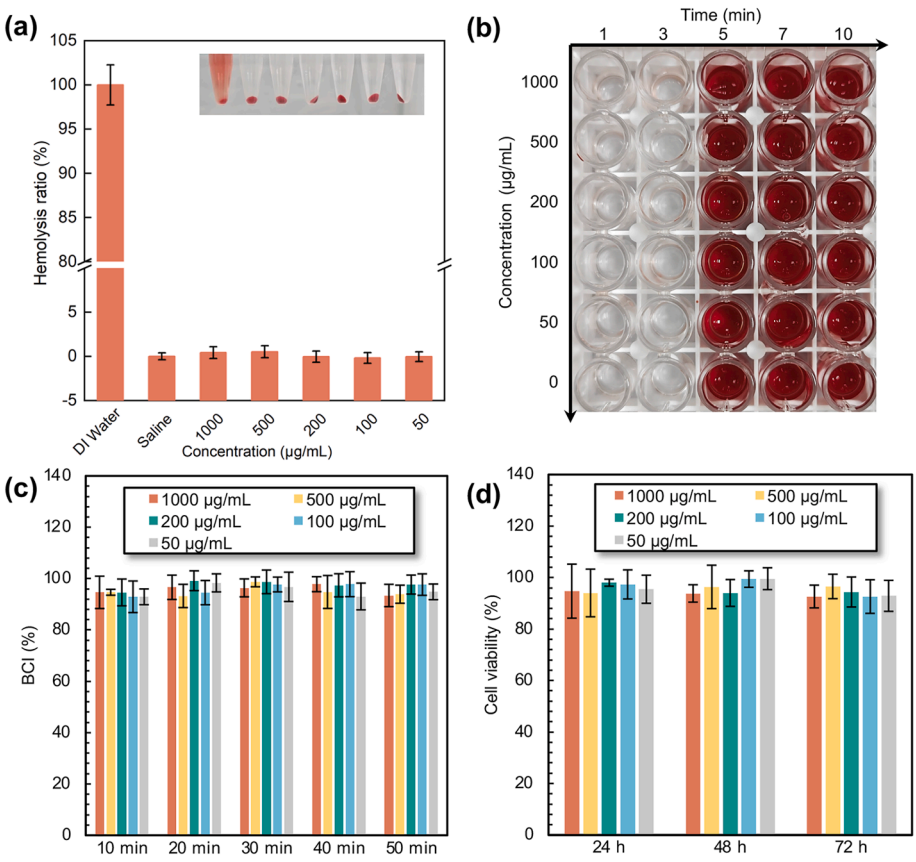

Fig. 5. (a) Hemolysis ratio of PCL_{42} microspheres. (b) Dynamic anticoagulation assay images of PCL_{42} microspheres. (c) BCI of PCL_{42} microspheres at different concentrations. (d) Cell viability of L929 cells co-cultured with PCL_{42} microspheres for 24, 48, and 72 h. Data are presented as mean ± SD from three independent experiments for each group.

respectively. The polydisperse $PCL_{ununiform}$ group shows a similar resolution pattern for erythema (resolving by day 6), but edematous nodules persist significantly longer, requiring 11 weeks for complete resolution. In the monodisperse PCL_{69} group, erythema and edema resolve by day 4 and week 3, respectively. By week 11, all inflammatory symptoms resolve in all experimental groups.

Notably, during the six-month observation period, the incidence and duration of persistent nodular formation are significantly higher in the polydisperse $PCL_{ununiform}$ group than in the monodisperse PCL_{42} and PCL_{69} groups. This chronic complication is likely attributable to the heterogeneous size distribution of $PCL_{ununiform}$ microspheres, which promotes microsphere agglomeration at the injection site. This localized clustering is hypothesized to increase local mechanical stress, which subsequently triggers the formation of a dense fibrotic capsule that encapsulated the aggregates, rendering the nodules resistant to resolution. Throughout the entire study, no mortality or severe adverse events are observed in any experimental rabbits, indicating good general tolerability of the injected PCL microsphere formulations.

3.5.2. *Histopathological analysis of host response*

As illustrated in Fig. S3, the histological section of the dorsal skin from the control group at week 24 exhibits the classic features of a healthy, homeostatic skin structure. The stratum corneum (horny layer) is significantly thickened, while the underlying stratified squamous epithelium (epidermis proper) is relatively thin, with keratinocytes arranged in a dense, regular and orderly manner. A distinct anatomical demarcation is clearly observed at the dermal-subcutaneous junction (indicated by the dashed line). To the left of this boundary is the subcutaneous adipose tissue (a loose connective tissue), while the structurally intact dermis, rich in organized extracellular matrix, resides to the right. Within the dermis, skin appendages such as hair follicles and sebaceous glands remain intact, and collagen fiber bundles form a well-defined, interwoven three-dimensional meshwork.

To systematically evaluate the host tissue response to the implanted PCL microspheres over time, we conduct histopathological scoring on H&E-stained paraffin sections obtained at 1, 2, 4, 8, 12, and 24 weeks post-implantation. This semi-quantitative assessment, based on established criteria for evaluating inflammatory and foreign body reactions, is used to grade the severity of tissue inflammatory responses in each experimental group.

As clearly depicted in Fig. 6(a), PCL microspheres are identifiable within the dermal layer. Notably, many microspheres exhibit deformation, a morphological artifact likely resulting from shear forces during the injection process, which induces microsphere compaction. Throughout the 24-week observation period, a mild inflammatory cell infiltrate, predominantly consisting of lymphocytes, is observed in all experimental groups. Compared to the untreated control skin, this represents a graded increase in the inflammatory response and associated fibrotic activity, indicating that the implantation of PCL microspheres elicits a typical, time-dependent foreign body reaction. In addition, to quantitatively assess the impact of PCL microspheres on dermal architecture, we conduct histomorphometric analysis on H&E-stained skin sections obtained at 1, 2, 4, 8, 12, and 24 weeks post-implantation. For each sample, the dermal thickness is manually measured at ten random non-overlapping locations by an operator blinded to grouping arrangements using CaseViewer software. The average thickness from these measurements is calculated to ensure statistical reliability.

The histopathological scoring data, summarized in Fig. 6(b), reveal distinct temporal patterns of the foreign body reaction, and the criteria for the four-point scoring scale is clarified in Supplementary Table S1.

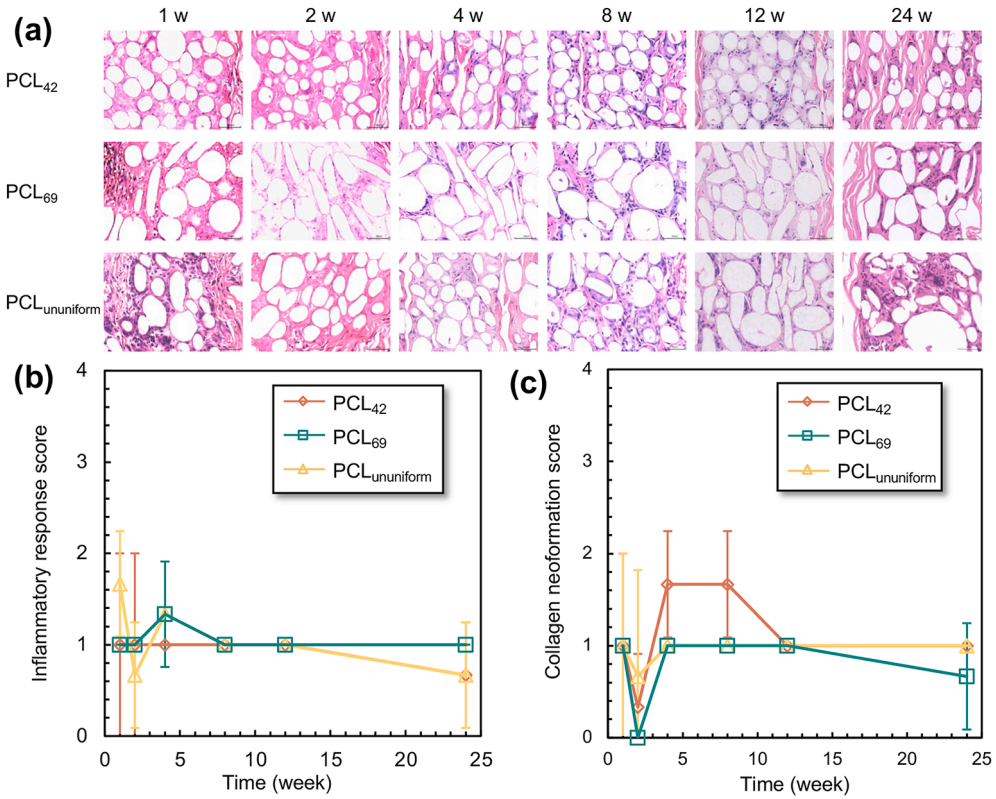

Fig. 6. (a) H&E staining images of the dermis and hypodermis at 1, 2, 4, 8, 12, 24 weeks after implantation of PCL microspheres. (b,c) Inflammatory response scores (b) and collagen neoformation scores (c) of subcutaneous tissue at 1, 2, 4, 8, 12, 24 weeks after implantation of PCL microspheres. Data are presented as mean ± SD from three independent experiments for each group.

The PCL_{42} group exhibits the most stable and favorable response, with a consistently low score of 1 from week 0 to 12, which gradually decreases to 0.67 by week 24, indicating resolving inflammation. In contrast, both the $PCL_{ununiform}$ and PCL_{69} groups exhibit a slightly enhanced initial inflammatory response within the first 4 weeks. However, by week 8, the inflammatory scores for all groups converge to a low and stable level, suggesting an innate self-limiting host response to the implanted microspheres.

Consistent with the inflammatory results, the assessment of collagen neogenesis (Fig. 6(c)) reveals a strong correlation between the materials' performance and their capacity to stimulate tissue regeneration. The PCL_{42} microspheres are the most potent in stimulating collagen production. The PCL_{69} group, however, induces a relatively weaker regenerative capacity. This difference may be attributed to the larger size of PCL_{69} microspheres, which could hinder cellular adhesion and proliferation, thereby impairing the activation of fibroblasts required for good matrix synthesis.

As illustrated in Fig. 7, all microsphere-treated groups exhibit a statistically significant increase in dermal thickness compared to the untreated control skin. Intriguingly, the magnitude of thickening shows a clear trend: PCL_{69} > PCL_{42} > $PCL_{uniform}$. This hierarchy in tissue response correlates directly with the average size of the respective microspheres, suggesting that the physical dimensions of the microspheres are a key determinant of their ability to induce tissue remodeling.

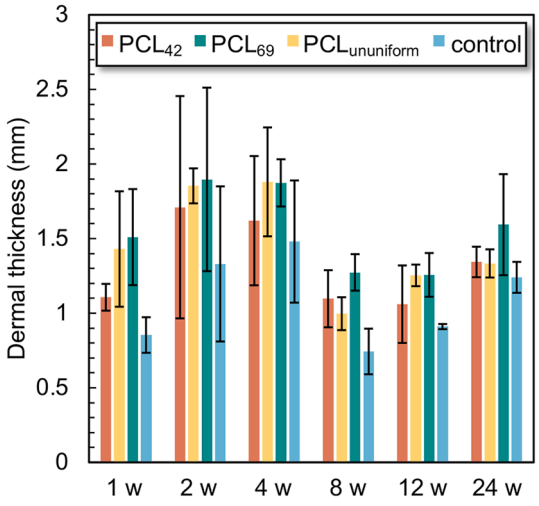

Fig. 7. Dermal thickness at 1, 2, 4, 8, 12, 24 weeks after implantation of PCL microspheres. Data are presented as mean ± SD from three independent experiments for each group.

3.5.3. *Tuning collagen neogenesis via PCL microspheres*

The dermal stromal compartment is primarily composed of two collagen isoforms: type I and type III. Type I collagen, the predominant structural protein of mature connective tissue, provides tensile strength and mechanical integrity to tissues such as the adult dermis, bone, and tendons via its densely packed fibrillar structure. In contrast, type III collagen forms delicate reticular networks primarily found in embryonic skin, vasculature, and mucosal tissues, endowing superior flexibility and elastic recoil.

Utilizing Picrosirius Red staining or immunofluorescence imaging, these collagen isoforms can be differentially visualized, with type I typically appearing as intense orange-red birefringent fibers (or red fluorescence), and type III exhibiting green birefringence/fluorescence. Qualitative analysis of the spatiotemporal collagen dynamics (Fig. 8(a)) reveals a dynamic shift in the regenerative response. During the initial 1-2 weeks post-implantation, the immediate pericapsular region is

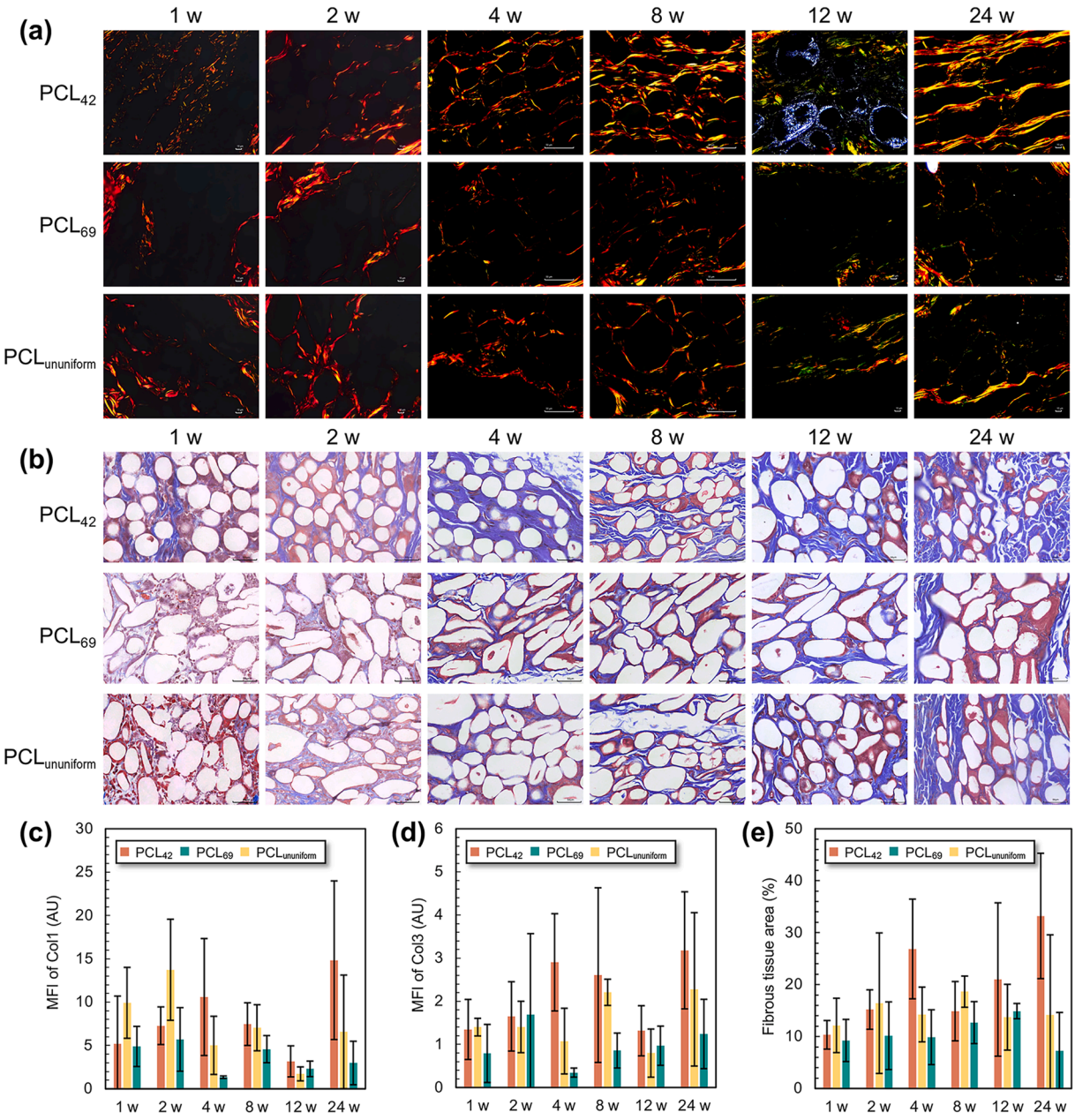

Fig. 8. (a) Sirius Red staining images of the dermis at 1, 2, 4, 8, 12, 24 weeks after implantation of PCL microspheres. (b) Masson's Trichrome staining images of the dermis at 1, 2, 4, 8, 12, 24 weeks after implantation. (c-e) MFI of Col I (c), MFI of Col III (d), and relative fibrous tissue area (e) of the dermis at 1, 2, 4, 8, 12, 24 weeks after implantation. Data are presented as mean ± SD from three independent experiments for each group.

dominated by a red fluorescent signal, indicative of nascent type I collagen production. From weeks 4 to 24, a gradual emergence of green fluorescence gradually emerges, representing type III collagen, suggesting a sequential wound-healing process. Tracing the intensity change of the type I collagen signal (red) over time provides further insights. In the PCL_{42} group, this signal progressively intensifies from weeks 1 to 8, diminishes at week 12, and undergoes a resurgence at week 24, indicating cyclic synthesis and remodeling. The $PCL_{ununiform}$ group exhibits a strong initial red signal at weeks 1-2, which subsequently wanes considerably. The PCL_{69} group consistently displays a comparatively weak red fluorescent signal throughout the study period, suggesting a reduced capacity for initiating good matrix synthesis.

Masson's Trichrome staining, a foundational histological method, is utilized to differentiate collagen fibers (blue-stained) from muscle/cytoplasm (red-stained) and nuclei (dark blue/black-stained), thereby enabling semi-quantitative assessment of collagen deposition and spatial distribution within the tissue. As illustrated in Fig. 8(b), the staining clearly depicts the temporal progression of the host response. At week 1, a sparse network of blue-stained collagen ensheathes the PCL_{42} microspheres, indicating an incipient fibrotic response. A significant shift occurs from week 4 onwards, with a pronounced deepening of blue staining evident around all three microsphere groups. This intensification signifies a phase of active neocollagenesis, where newly synthesized collagen fibers are deposited at the implantation site. By weeks 12 and 24, the PCL_{42} group exhibits a markedly denser and more extensive blue-stained collagen matrix surrounding the microspheres compared to the $PCL_{ununiform}$ and PCL_{69} groups. This observation suggests a superior capacity of the monodisperse PCL_{42} microspheres to promote sustained and abundant collagen production, leading to enhanced host tissue integration.

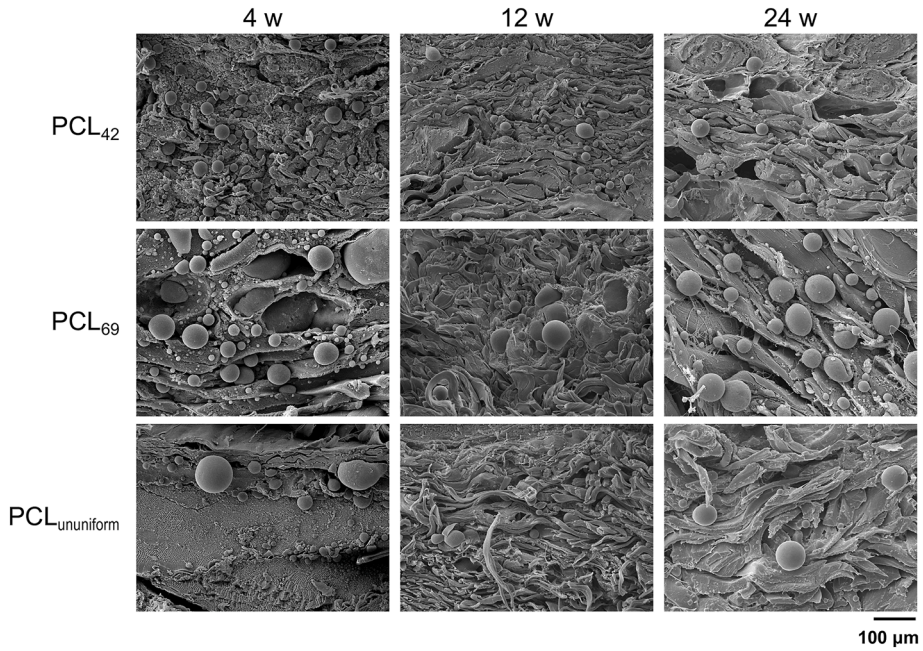

Fig. 9. SEM images of PCL_{42}, PCL_{69}, $PCL_{ununiform}$ microspheres at 4, 12, 24 weeks after implantation.

3.5.4. Semi-quantitative analysis of collagen density

The temporal evolution of collagen expression serves as a definitive fingerprint of the regenerative versus fibrotic trajectory. Our data (Fig. 8 (c–e)) unveil a conserved triphasic pattern across all microsphere groups, a manifestation of the host's wound healing program modulated by the implanted microspheres. The regeneration of collagen may undergo the following three stages. Phase 1 (weeks 1-2): An initial collagen surge is a hallmark of the inflammatory phase, where macrophage-secreted factors drive fibroblast activation to form a matrix scaffold. Phase 2 (weeks 4-8): A subsequent decline is indicative of an active remodeling phase, likely triggered by a localized acidic microenvironment derived from PCL polymer degradation. This pH shift plausibly induces the activation of matrix metalloproteinases (MMPs), enzymes that actively degrade the nascent matrix to prepare for organized tissue reconstruction. Phase 3 (weeks 12-24): The final ascent signifies the maturation phase, wherein persistent physical cues from the microspheres sustain fibroblast engagement, culminating in the synthesis of a functional and stable collagen network.

Critically, the magnitude of this regenerative response is significantly influenced by microsphere size. The PCL_{69} group's blunted collagen response suggests that excessively large microspheres induce a hostile, poorly vascularized microenvironment, severely impairing cellular crosstalk and matrix synthesis. A pivotal temporal insight emerges when comparing PCL_{42} and $PCL_{ununiform}$: while $PCL_{ununiform}$ initiates a stronger early inflammatory response driven by acute, heterogeneous PCL degradation, PCL_{42} demonstrates superior long-term performance. We attribute this to its monodisperse nature, which enables predictable and gradual degradation kinetics. This generates a tempered, sustained inflammatory signal that favors the recruitment and function of regenerative fibroblasts over destructive inflammatory cells, thereby facilitating a superior regenerative outcome over time.

3.5.5. Physical stability and structural integrity of PCL microspheres in rabbit models

To directly assess the *in vivo* stability and morphological integrity of the implanted PCL microspheres, we harvest full-thickness dermal tissue samples containing the microspheres at 4, 12, and 24 weeks post-implantation. These samples are processed for SEM, enabling in situ characterization of the microspheres' morphology and surface topography.

As shown in Fig. 9, representative SEM images demonstrate that PCL_{42}, PCL_{69}, and $PCL_{ununiform}$ microspheres maintain their original spherical morphology and smooth surface throughout the 24-week observation period. No obvious signs of surface erosion, pitting, fragmentation, or bulk degradation are observed in any microsphere group. These observations confirm that PCL microspheres possess exceptional *in vivo* stability in the rabbit model, with negligible degradation over the study period. This notable *in vivo* persistence highlights their potential as implantable biomaterials for long-term therapeutic applications.

4. Conclusion

In this study, we successfully fabricate PCL microspheres with desirable properties for soft tissue augmentation using a microfluidic technique. The sizes of O/W droplet templates and the resulting PCL microspheres are regulable by simply adjusting the outer-to-inner phase flow rate ratio, yielding highly monodisperse microspheres with a CV value consistently below 5%. We further investigate the influence of PCL concentration in the inner phase (1 wt%, 3 wt%, and 5 wt%) on microsphere formation, revealing a concentration-dependent decrease in the diameter shrinkage ratio during solidification (75.73%, 67.20%, and 60.36%, respectively), while their microscopic morphology remains unaffected. Importantly, the prepared PCL microspheres exhibit excellent *in vitro* stability, with no significant alterations in size or morphology after 8 weeks of degradation, alongside favorable biocompatibility as evidenced by low hemolysis rates (<1%), high BCI (>90%), and high cell viability (>85% in CCK-8 assays). *In vivo* implantation studies in rabbits demonstrate that these microspheres, regardless of their size uniformity (e.g., PCL_{42}, PCL_{69}, $PCL_{ununiform}$), induce only mild local inflammatory responses. More significantly, all tested microspheres promote collagen regeneration to varying degrees, as confirmed by Sirius Red and Masson's trichrome staining. Notably, among these, the monodisperse PCL microspheres with an average size of 42 μm exhibit superior performance in mitigating inflammation and stimulating collagen deposition compared to polydisperse or larger-sized microspheres. Collectively, our findings demonstrate that

monodisperse PCL microspheres, particularly those with an optimized size (~42 μm), possess a unique combination of controllable size, excellent stability, favorable biocompatibility, and good pro-regenerative capacity. These attributes strongly support their potential as promising candidates for soft tissue augmentation applications in the field of medical aesthetics.

CRediT authorship contribution statement

Xing-Long Zhou: Writing – original draft, Validation, Investigation, Funding acquisition, Conceptualization. **Hao-Wen Zhu:** Methodology, Formal analysis, Data curation. **Han Fu:** Methodology. **Chang-Hai Zhou:** Visualization. **Da-Wei Pan:** Methodology. **Yu-Chao Deng:** Methodology. **Wei Wang:** Methodology. **Zhuang Liu:** Methodology. **Rui Xie:** Methodology. **Xiao-Jie Ju:** Writing – review & editing, Supervision, Methodology, Funding acquisition, Conceptualization. **Liang-Yin Chu:** Supervision, Methodology.

Declaration of competing interest

The authors declare that they have no known competing financial interests or personal relationships that could have appeared to influence the work reported in this paper.

Acknowledgments

The authors gratefully acknowledge support from the National Natural Science Foundation of China (grant Nos. 22494713 and 22308229).

Appendix A. Supplementary data

Supplementary data to this article can be found online at https://doi.org/10.1016/j.partic.2026.04.027.

References

Bai, L., Guo, C., Cao, S., Zhang, X., Li, X., Fang, Q., Zhang, Y., & Xu, G. (2025). A novel injectable sericin/nano-hydroxyapatite hydrogel as a dermal filler for soft tissue augmentation. *International Journal of Biological Macromolecules, 320*, Article 145814. https://doi.org/10.1016/j.ijbiomac.2025.145814

Cao, M., Tao, L., Zhang, Y., Zhou, L., Wu, S., Zhou, H., Ge, Y., Zou, Y., & Luo, S. (2025). Increasing collagen synthesis in fibroblasts: The roles of PCL microspheres and the SAMD11-PLOD1 axis in skin rejuvenation. *Biochimica et Biophysica Acta - Molecular Cell Research, 1872*(4), Article 119931. https://doi.org/10.1016/j.bbamcr.2025.119931

Carretero, V. J., Ramos, E., Segura-Chama, P., Hernández, A., Baraibar, A. M., Álvarez-Merz, I., Muñoz, F. L., Egea, J., Solís, J. M., Romero, A., & Hernández-Guijo, J. M. (2023). Non-excitatory amino acids, melatonin, and free radicals: Examining the role in stroke and aging. *Antioxidants, 12*(10), 1844. https://doi.org/10.3390/antiox12101844

Chikaura, H., Nakashima, Y., Fujiwara, Y., Komohara, Y., Takeya, M., & Nakanishi, Y. (2016). Effect of particle size on biological response by human monocyte-derived macrophages. *Biosurface and Biotribology, 2*(1), 18–25. https://doi.org/10.1016/j.bsbt.2016.02.003

Choi, W. I., Hwang, Y., Sahu, A., Min, K., Sung, D., Tae, G., & Chang, J. H. (2018). An injectable and physical levan-based hydrogel as a dermal filler for soft tissue augmentation. *Biomaterials Science, 6*(10), 2627–2638. https://doi.org/10.1039/C8BM00524A

Chu, L. Y., Utada, A. S., Shah, R. K., Kim, J. W., & Weitz, D. A. (2007). Controllable monodisperse multiple emulsions. *Angewandte Chemie International Edition, 46*(47), 8970–8974. https://doi.org/10.1002/anie.200701358

Deliormanli, A. M., & Yenice, A. C. (2021). Preparation of hollow PCL microspheres by o/w single emulsion-solvent evaporation method in the presence of graphene nanopowders. *Express Polymer Letters, 15*(7), 641–653. https://doi.org/10.3144/expresspolymlett.2021.54

Fan, H., & Jin, Z. (2015). Hierarchical porous polycaprolactone microspheres generated via a simple pathway combining nanoprecipitation and hydrolysis. *Chemical Communications, 51*(82), 15114–15117. https://doi.org/10.1039/C5CC04586J

Gao, Q., Duan, L., Feng, X., & Xu, W. (2021). Superiority of poly(L-lactic acid) microspheres as dermal fillers. *Chinese Chemical Letters, 32*(1), 577–582. https://doi.org/10.1016/j.cclet.2020.03.071

Herrmann, J. L., Hoffmann, R. K., Ward, C. E., Schulman, J. M., & Grekin, R. C. (2018). Biochemistry, physiology, and tissue interactions of contemporary biodegradable injectable dermal fillers. *Dermatologic Surgery, 44*, S19–S31. https://doi.org/10.1097/DSS.0000000000001582

Hossain, K. M. Z., Patel, U., & Ahmed, I. (2015). Development of microspheres for biomedical applications: A review. *Progress in Biomaterials, 4*(1), 1–19. https://doi.org/10.1007/s40204-014-0033-8

Hua, Y., Ma, C., Wei, T., Zhang, L., & Shen, J. (2020). Collagen/chitosan complexes: Preparation, antioxidant activity, tyrosinase inhibition activity, and melanin synthesis. *International Journal of Molecular Sciences, 21*(1), 313. https://doi.org/10.3390/ijms21010313

Hwang, Y., Lee, J. S., An, H., Oh, H., Sung, D., Tae, G., & Choi, W. I. (2021). Hydroxyapatite-embedded levan composite hydrogel as an injectable dermal filler for considerable enhancement of biological efficacy. *Journal of Industrial and Engineering Chemistry, 104*, 491–499. https://doi.org/10.1016/j.jiec.2021.08.040

Ikada, Y., & Tsuji, H. (2000). Biodegradable polyesters for medical and ecological applications. *Macromolecular Rapid Communications, 21*(3), 117–132. https://doi.org/10.1002/(SICI)1521-3927(20000201)21:3<117::AID-MARC117>3.0.CO;2-X

Jang, H. Y., Shin, J. Y., Oh, S. H., Byun, J. H., & Lee, J. H. (2020). PCL/HA hybrid microspheres for effective osteogenic differentiation and bone regeneration. *ACS Biomaterials Science & Engineering, 6*(9), 5172–5180. https://doi.org/10.1021/acsbiomaterials.0c00550

Jeong, S. H., Fan, Y. F., Baek, J. U., Song, J., Choi, T. H., Kim, S. W., & Kim, H. E. (2016). Long-lasting and bioactive hyaluronic acid-hydroxyapatite composite hydrogels for injectable dermal fillers: Physical properties and in vivo durability. *Journal of Biomaterials Applications, 31*(3), 464–474. https://doi.org/10.1177/0885328216648809

Jiang, Q. R., Pu, X. Q., Deng, C. F., Wang, W., Liu, Z., Xie, R., Pan, D. W., Zhang, W. J., Ju, X. J., & Chu, L. Y. (2023). Microfluidic controllable preparation of iodine-131-labeled microspheres for radioembolization therapy of liver tumors. *Advanced Healthcare Materials, 12*(21), Article 2300873. https://doi.org/10.1002/adhm.202300873

Kontis, T. C. (2013). Contemporary review of injectable facial fillers. *JAMA Facial Plastic Surgery, 15*(1), 58–64. https://doi.org/10.1001/jamafacial.2013.337

Li, J., Xu, J., Wang, Y., Chen, Y., Ding, Y., Gao, W., Tan, Y., Ge, N., Chen, Y., Ge, S., Yang, Q., He, B., & Ye, X. (2024a). Fusible and radiopaque microspheres for embolization. *Advanced Materials, 36*(39), Article 2405224. https://doi.org/10.1002/adma.202405224

Li, X., Liao, X., Jia, Z., Liu, S., Li, P., Li, L., Zhang, W., Niu, X., & Fan, Y. (2024b). Biodegradable PLLA/PLGA microspheres/collagen composites for continuous soft tissue augmentation. *Composites Part B: Engineering, 283*, Article 111603. https://doi.org/10.1016/j.compositesb.2024.111603

Li, Y., Zha, Y., Hu, W., Chen, J., Liu, S., Zhang, S., & Wang, J. (2023). Monoporous microsphere as a dynamically movable drug carrier for osteoporotic bone remodelling. *Advanced Healthcare Materials, 12*(16), Article 2201242. https://doi.org/10.1002/adhm.202201242

Long, Y. H., Ju, X. J., Yang, S. H., Chen, S. K., Xie, R., Wang, W., Liu, Z., Pan, D. W., & Chu, L. Y. (2024). Microfluidic fabrication of monodisperse hyaluronic acid microspheres with excellent biocompatibility and tunable physicochemical properties. *Industrial & Engineering Chemistry Research, 63*(15), 6632–6643. https://doi.org/10.1021/acs.iecr.4c00337

Minokadeh, A., & Kakar, R. (2025). The history of dermal fillers in dermatologic surgery. *Dermatologic Surgery, 51*(5), 465–470. https://doi.org/10.1097/DSS.0000000000004650

Nakamura, R., Uehara, S., Suematsu, K., Ishitsuka, Y., & Noma, H. (2021). Prediction of future wrinkles for middle-aged women: A 7-year longitudinal study on the progression of wrinkles in Japanese women. *Skin Research and Technology, 27*(5), 854–862. https://doi.org/10.1111/srt.13031

Pan, Y., Xiao, Y., Hao, Y., Shi, K., Pan, M., & Qian, Z. (2022). An injectable mPEG-PDLLA microsphere/PDLLA-PEG-PDLLA hydrogel composite for soft tissue augmentation. *Chinese Chemical Letters, 33*(5), 2486–2490. https://doi.org/10.1016/j.cclet.2021.12.093

Requena, L., Requena, C., Christensen, L., Zimmermann, U. S., Kutzner, H., & Cerroni, L. (2011). Adverse reactions to injectable soft tissue fillers. *Journal of the American Academy of Dermatology, 64*(1), 1–34. https://doi.org/10.1016/j.jaad.2010.02.064

Seong, Y. J., Lin, G., Kim, B. J., Kim, H. E., Kim, S., & Jeong, S. H. (2019). Hyaluronic acid-based hybrid hydrogel microspheres with enhanced structural stability and high injectability. *ACS Omega, 4*(9), 13834–13844. https://doi.org/10.1021/acsomega.9b01475

Shin, J. W., Kwon, S. H., Choi, J. Y., Na, J. I., Huh, C. H., Choi, H. R., & Park, K. C. (2019a). Molecular mechanisms of dermal aging and antiaging approaches. *International Journal of Molecular Sciences, 20*(9), 2126. https://doi.org/10.3390/ijms20092126

Shin, S. W., Jang, Y. D., Ko, K. W., Kang, E. Y., Han, J. H., Bedair, T. M., Kim, I. H., Son, T. I., Park, W., & Han, D. K. (2019b). PCL microspheres containing magnesium hydroxide for dermal filler with enhanced physicochemical and biological performances. *Journal of Industrial and Engineering Chemistry, 80*, 854–861. https://doi.org/10.1016/j.jiec.2019.07.043

Varani, J., Dame, M. K., Rittie, L., Fligiel, S. E. G., Kang, S., Fisher, G. J., & Voorhees, J. J. (2006). Decreased collagen production in chronologically aged skin - Roles of age-dependent alteration in fibroblast function and defective mechanical stimulation. *American Journal of Pathology, 168*(6), 1861–1868. https://doi.org/10.2353/ajpath.2006.051302

Wang, H., Li, W., & Li, Z. (2018). Preparation of fluorinated PCL porous microspheres and a super-hydrophobic coating on fabrics via electrospraying. *Nanoscale, 10*(39), 18857–18868. https://doi.org/10.1039/C8NR05793A

Wen, S., Ju, X. J., Liu, W. Y., Liu, Y. Q., Pu, X. Q., Liu, Z., Wang, W., Xie, R., Faraja, Y., & Chu, L. Y. (2023). Ca-alginate-based Janus capsules with pumping effect for intestinal-targeted controlled-release. *Engineering, 24*, 114–125. https://doi.org/10.1016/j.eng.2022.05.021

Xie, D., Che, X., Zha, L., Zhang, Q., Chen, M., & Wang, L. (2025). Astragaloside-loaded PCL microspheres prepared from microchips for promoting collagen regenerating. *Journal of Biomaterials Science-Polymer Edition*, 1–19. https://doi.org/10.1080/09205063.2025.2604821

Yan, H., Wang, Q., Li, W., Li, N., Huang, P., & Xiao, J. (2024). Injectable and biodegradable collagen–chitosan microspheres for enhanced skin regeneration. *Journal of Materials Chemistry B, 12*(35), 8757–8766. https://doi.org/10.1039/D4TB00537F

Yan, B., Wang, X., Zhang, X., Liu, S., Lu, H., & Ran, R. (2022). One-step preparation of hydroxyapatite-loaded magnetic polycaprolactone hollow microspheres for malachite green adsorption by Pickering emulsion template method. *Colloids and Surfaces A: Physicochemical and Engineering Aspects, 639*, Article 128347. https://doi.org/10.1016/j.colsurfa.2022.128347

Yang, S. H., Song, W. L., Fan, L. L., Deng, C. F., Xie, R., Wang, W., Liu, Z., Pan, D. W., Ju, X. J., & Chu, L. Y. (2024). Microfluidic fabrication of monodisperse microcapsules with gas cores. *Lab on a Chip, 24*(14), 3556–3567. https://doi.org/10.1039/D4LC00443D